Gas Phase Selective Hydrogenation of Phenylacetylene to Styrene over Au/Al_2O_3

Xiaodong Wang[a,b,*] and Mark A. Keane[a]

[a]Chemical Engineering, School of Engineering & Physical Sciences, Heriot-Watt University, Edinburgh EH14 4AS, Scotland

[b]Chemical and Materials Engineering, School of Engineering, University of Aberdeen, Aberdeen AB24 3UE, Scotland

*corresponding author

Tel: +44(0)1224 273 956, e-mail: x.wang@abdn.ac.uk

ABSTRACT

BACKGROUND: Trace quantities of phenylacetylene can poison styrene polymerisation catalysts. The phenylacetylene content must be less than 10 ppm and selective hydrogenation (to styrene) is viewed as a viable process solution. High styrene selectivities have been achieved in batch liquid phase operations while a switch from conventional batch liquid to continuous gas phase reaction presents process advantages in terms of higher throughput and enhanced productivity. We aim to provide the first direct comparison of Au/Al_2O_3 and Pd/Al_2O_3 in gas phase continuous catalytic hydrogenation of phenylacetylene.

RESULTS: TPR reduction generated metal particles at the nano-scale (mean size = 3.0-4.3 nm), with evidence of electron donation from the Al_2O_3 carrier. Pd/Al_2O_3 exhibited a greater specific H_2 uptake capacity than Au/Al_2O_3 under reaction conditions to deliver appreciably higher turnover frequencies (TOF) for reaction in excess H_2. Stepwise hydrogenation predominated over Au/Al_2O_3 with 100% selectivity to styrene at 353 K where an increase in temperature favoured subsequent hydrogenation to ethylbenzene. Under the same conditions, Pd/Al_2O_3 was non-selective, activating styrene to generate ethylbenzene with a greater contribution of direct phenylacetylene hydrogenation to ethylbenzene at higher temperature.

CONCLUSION: Kinetic analysis has revealed stepwise phenylacetylene hydrogenation in excess H_2 over Au/Al_2O_3 with 100% selectivity to styrene. Stepwise hydrogenation also prevailed over Pd/Al_2O_3 at the lower temperature but surface activation of styrene coupled with enhanced H_2 dissociation generated significant ethylbenzene. Decreasing inlet H_2/phenylacetylene (to 1 mol/mol) over Pd/Al_2O_3 lowered rate where the activity/selectivity profile overlapped that exhibited by Au/Al_2O_3 in excess H_2.

1. Introduction

Trace quantities of phenylacetylene can poison styrene polymerisation catalysts.[1,2] The phenylacetylene content must be less than 10 ppm[3] and selective hydrogenation (to styrene) is viewed as a viable process solution.[2,4] High styrene selectivities have been achieved in batch liquid phase operations using Pd based catalysts.[5,6] Bacchi *et al.* reported 92% styrene yield for reaction over Pd complexes (with hydrazine ligands)[5] while the application of Pd/MCM-41 delivered a 96% yield.[6] Other transition metal (Ru,[7] Pt,[7] Rh[8] and Ni[9]) catalysts are active in this reaction with varying levels of selectivity. In terms of reaction pathway, it has been established (in liquid phase operation) that phenylacetylene undergoes consecutive reduction where styrene serves as an intermediate in the subsequent conversion to ethylbenzene.[10-12] Liu *et al.* have demonstrated by FTIR analysis that selectivity is sensitive to H_2/phenylacetylene ratio where styrene is favoured under H_2 lean conditions.[12]

A switch from conventional batch liquid to continuous gas phase reaction presents process advantages in terms of higher throughput and enhanced productivity. Indeed, Goršek and Glavič in their assessment of production rate and energy integration concluded that a continuous plant is more profitable than one employing batch reactions for all capacities.[13] Gas phase continuous operation circumvents down time (between batches) and the use of additional chemicals as solvents, hydrogen donors and derivatisation agents.[14-16] Reported gas phase phenylacetylene hydrogenation is limited to the work of Nilolaev *et al.* who examined the application of Au/Al_2O_3 in the conversion of phenylacetylene/styrene mixtures.[17-19] Selectivity to styrene was below 30% and activity was dependent on Au particle size (2.5-30 nm).[17,18] There is considerable scope to enhance Au promoted styrene production in continuous

operation. In previous work, we have demonstrated 100% selectivity in the hydrogenation of functionalised nitroarenes over oxide supported Au to target amine products[20-22] and in the conversion of benzaldehyde to benzyl alcohol.[23] We have now extended that work to consider the catalytic action of Au/Al_2O_3 in selective phenylacetylene → styrene, assessing the effects of temperature and H_2 partial pressure as critical process variables. Drawing on the published liquid phase catalytic work where supported Pd was the predominant catalyst system,[4,6,24-27] we have employed Pd/Al_2O_3 as benchmark and correlate catalyst testing with structural characterisation.

2. Materials and Methods

2.1 Catalyst Preparation

A 1.1% w/w $Au/\gamma\text{-}Al_2O_3$ was prepared by deposition-precipitation. Urea, used as basification agent, was added (100-fold excess) to a solution of $HAuCl_4$ (4.4×10^{-2} M), the $\gamma\text{-}Al_2O_3$ support (Puralox, Condea Vista Co.) was introduced and the suspension stirred and heated to 353 K (2 K min^{-1}) for 3 h. The pH progressively increased to reach *ca.* 7 after 3 h as a result of urea decomposition

$$NH_2\text{-}CO\text{-}NH_2 + 3H_2O \xrightarrow{T=353K} 2NH_4^+ + 2OH^- + CO_2 \qquad (1)$$

The resultant solid was separated by centrifugation, washed repeatedly with deionised water (with centrifugation between each washing) until the washing water was Cl-free (based on the $AgNO_3$ test) and dried in He (45 cm^3 min^{-1}) at 373 K (2 K min^{-1}) for 5 h. For comparison purposes, a commercial (Sigma-Aldrich) 1.2 % w/w Pd/Al_2O_3 catalyst was employed and used as received. The catalysts were sieved to 75 μm average particle diameter (ATM fine test sieves) and the Au and Pd loadings determined by inductively coupled plasma-optical emission

spectrometry (ICP-OES, Vista-PRO, Varian Inc.) from the diluted extract of aqua regia.

2.2 Catalyst Characterisation

Nitrogen adsorption-desorption isotherms were measured at 77 K using the commercial automated Micromeritics Gemini 2390 system; samples were outgassed at 423 K under N_2 for 1 h prior to analysis. Specific surface areas were calculated using the standard BET method with mean pore size and cumulative pore volumes determined by BJH analysis of the desorption isotherms. Temperature programmed reduction (TPR) and H_2 chemisorption were recorded using the commercial CHEMBET 3000 (Quantachrome Instrument) unit; data acquisition/manipulation employed the TPR Win^{TM} software. The samples were loaded into a U-shaped quartz cell (100 mm × 3.76 mm i.d.) and heated in 17 cm^3 min^{-1} (Brooks mass flow controlled) 5% v/v H_2/N_2 to 573 K (Pd/Al_2O_3) or 603 K (Au/Al_2O_3) at 2 K min^{-1}. The effluent gas passed through a liquid N_2 trap and H_2 consumption was monitored by a thermal conductivity detector. Post-TPR, samples were swept with 65 cm^3 min^{-1} N_2 for 1.5 h, cooled to 423 K or 298 K and subjected to H_2 chemisorption by pulse (10-50 µl) titration.

Powder x-ray diffractograms (XRD) were recorded on a Bruker/Siemens D500 incident x-ray diffractometer using Cu Kα radiation. Samples were scanned at 0.02º $step^{-1}$ over the range $20º \leq 2\theta \leq 85º$ and the diffractograms were compared with JCPDS-ICDD reference standards (Au (Card No. 04-0784), Pd (05-0681) and γ-Al_2O_3 (10-0425)). Metal (Au and Pd) particle morphology and size were determined by transmission (TEM, JEOL JEM 2011) and scanning transmission electron microscopy (STEM, JEOL 2200FS) electron microscopy, employing Gatan DigitalMicrograph 1.82 for data acquisition/manipulation. Samples for analysis were prepared by dispersion in acetone and deposited on a holey carbon/Cu grid (300 Mesh). The

surface area-weighted metal diameter (d_{TEM}) was calculated from

$$d_{TEM} = \frac{\sum_i n_i d_i^3}{\sum_i n_i d_i^2} \quad (2)$$

where n_i is the number of particles of diameter d_i and $\Sigma n_i > 200$. X-ray photoelectron spectroscopy (XPS) analysis was conducted on an Axis Ultra instrument (Kratos Analytical) under ultra-high vacuum (< 10^{-8} Torr) using a monochromatic Al Kα X-ray source (1486.6 eV). Analyser pass energy was 80 eV for survey (0–1000 eV) and 40 eV for high resolution spectra (Au $4f_{7/2}$ and Pd $3d_{5/2}$). The adventitious carbon 1*s* peak at 284.5 eV was used as internal standard to compensate for any charging effects. Spectra curve fitting and quantification were performed with the Casa XPS software, using relative sensitivity factors provided by Kratos.

2.3 Catalytic Procedure

Reactions were carried out at H_2 partial pressures in the range 1.5×10^{-3}– 0.88 atm (varied by dilution in He, total pressure = 1 atm), immediately after *in situ* reduction (at 2 K min^{-1} to 573-603 K in 60 cm^3 min^{-1} H_2 for 1h) in a continuous flow fixed bed vertical glass reactor (i.d. = 15 mm, *l* = 600 mm) at 353-473 K. The catalytic reactor and operating conditions to ensure negligible heat/mass transport limitations have been fully described elsewhere[28,29] but features pertinent to this study are given below. A layer of borosilicate glass beads served as preheating zone, ensuring that the inlet phenylacetylene (or styrene) was vaporised and reached reaction temperature before contacting the catalyst. Isothermal conditions (±1 K) were ensured by diluting the catalyst bed with ground glass (75 μm). Temperature was continuously monitored by a thermocouple inserted in a thermowell within the catalyst bed. Phenylacetylene (or styrene) was delivered *via* a glass/teflon air-tight syringe and teflon line using a microprocessor

controlled infusion pump (Model 100 kd Scientific) at a fixed calibrated flow rate. A co-current flow of H_2 (or H_2/He) was maintained at $GHSV = 2\times10^4$ h^{-1} with an inlet organic flow (F) of 0.6×10^{-4}–4.8×10^{-3} mol h^{-1}; molar metal (n) to F ratio spanned the range 2.3×10^{-5}–4.7×10^{-2} h. At the low partial pressures of phenylacetylene in the feed, thermochemical calculations have confirmed that the reactant is in the gas phase over the temperature range applied. In blank tests, passage of phenylacetylene (or styrene) in H_2 through the empty reactor or over the support alone did not result in any detectable conversion. The reactor effluent was frozen in a liquid N_2 trap for subsequent analysis, using a Perkin-Elmer Auto System XL gas chromatograph equipped with a programmed split/splitless injector and FID, employing a DB-1 50 m × 0.20 mm i.d. 0.33 μm film thickness capillary column (J&W Scientific), as described elsewhere.[30] Phenylacetylene (Aldrich, ≥ 99.9%), styrene (Aldrich, ≥ 99.9%) and ethanol (Riedel-de Häen, ≥ 99.5%) as carrier were used without further purification. Repeated reactions with different samples from the same batch of catalyst delivered raw conversion and selectivity data that were reproducible to within ±6 %. Turnover frequency (*TOF*) was calculated based on Au and Pd dispersion obtained from TEM/STEM analysis.

3. Results and Discussion

3.1 Au/Al_2O_3

3.1.1 Catalyst Characteristics

Critical Au/Al_2O_3 characteristics are given in Table 1. The BET surface area (166 m^2 g^{-1}), total pore volume (0.36 cm^3 g^{-1}) and mean size (5.8 nm) are within the range (150–250 m^2 g^{-1}, 0.27–0.75 cm^3 g^{-1} and 3.5–15 nm) reported for γ-Al_2O_3 supported metal systems.[31,32] Catalyst activation by temperature programmed reduction (TPR) generated the profile shown in Fig.

1(A), exhibiting a positive signal with T_{max} = 458 K. The associated H_2 consumption (87 µmol g^{-1}) matches that required for the reduction of the precursor to the metallic state (84 µmol g^{-1}), *i.e.* $Au^{3+} \rightarrow Au^0$. A single TPR peak has been reported previously for Au/Al_2O_3 at 434 K[33] and 503 K.[34] XPS measurements were conducted to probe Au electronic character and the resultant spectrum over the Au 4*f* binding energy (BE) region is given in Fig. 1(B). The extracted Au $4f_{7/2}$ BE (83.4 eV) is significantly lower than that reported for metallic Au (84.0 eV),[35] suggesting electron transfer from the support to generate electron rich $Au^{\delta-}$, as has been proposed for Au on Al_2O_3.[36,37]

Hydrogenation activity is dependent on H_2 activation where dissociative chemisorption occurs on low coordination Au sites.[38] Hydrogen uptake is enhanced with decreasing Au particle size at the nano-scale due to the preponderance of Au corner and edge sites.[39] XRD analysis (diffractogram not shown) only revealed peaks due to the support, suggesting a well dispersed supported Au phase. We have applied STEM analysis to determine Au size (distribution and mean) and the representative image (Fig. 1(C)) demonstrates the occurrence of pseudo-spherical Au particles in the size range 2-8 nm with a surface area weighted mean size of 4.3 nm; see size distribution histogram in Fig. 1(C). Hydrogen uptake measured at ambient temperature (Table 1) was low suggesting limited capacity to chemisorb H_2, as has been noted elsewhere for a range of Au systems.[25,40,41] Uptake was appreciably higher at 423 K (median reaction temperature), indicating that H_2 chemisorption on supported Au is an activated process. Although we could find no reported chemisorption values to relate to our measurements, van Bokhoven and co-workers[39,42] and Lin *et al*.[43] have proposed enhanced H_2 activation on Au/Al_2O_3 and Au/TiO_2, respectively, at higher temperatures.

3.1.2 Catalytic Response

The consecutive phenylacetylene hydrogenation to ethylbenzene *via* styrene[11,12] is shown in Fig. 2 (reaction *via* steps II and III), which also includes a parallel direct route (step I). Fractional phenylacetylene conversion (x) is illustrated as a function of time on-stream at two reaction temperatures in the inset to Fig. 2. The temporal variation in activity can be expressed in terms of the empirical relationship[33,37]

$$\frac{(x - x_0)}{(x_{3h} - x_0)} = \frac{\Delta t}{(\beta + \Delta t)} \tag{3}$$

where x_{3h} represents conversion after 3 h on-stream and β is a time scale fitting parameter. Fit convergence yielded x_0 (initial conversion), which was used to obtain the turnover frequencies (*TOF*, rate normalised per surface Au site) given in Table 2. Reaction over Au/Al_2O_3 delivered exclusive styrene production at 353 K (x = 0.1). This is a significant result as there has been no reported instance of 100% styrene selectivity in gas phase continuous operation. An increase in reaction temperature (from 353 to 473 K) resulted in an order of magnitude increase in *TOF*, generating styrene as principal product with secondary formation of ethylbenzene (Table 2). A shift in selectivity to ethylbenzene at higher temperatures (up to 343 K) has also been observed in the liquid phase over carbon supported Pd and Pt catalysts.[3,44] The extended activity/selectivity response is shown in Fig. 3. High styrene selectivity (> 90%) was maintained at 353 K but there was a clear decline at 473 K with increasing conversion, consistent with a stepwise mechanism (steps II and III in Fig. 2). Styrene and ethylbenzene were the only detected products with no evidence of dealkylation (to toluene) or condensation steps as reported for reaction over Ni and Ni-Pd catalysts.[9] We can note high alkene selectivities obtained with Au/Al_2O_3 in the hydrogenation of acetylene,[45,46] propyne[47] and 1,3-butadiene.[48]

Use of styrene as reactant generated ethylbenzene as the sole product but with an appreciably lower *TOF* relative to that recorded with phenylacetylene as feed (Table 2). This can account for the observed styrene selectivity from phenylacetylene where subsequent hydrogenation proceeded at a far lower rate. As both phenylacetylene and styrene act as Lewis bases, interaction with the Lewis acid-base sites on Al_2O_3 ($Al^{\delta+}$–$O^{\delta-}$) can lead to dissociative adsorption through the terminal carbon atom at $Al^{\delta+}$ with a proton bonded to the adjacent $O^{\delta-}$. Ivanov *et al.* have provided evidence from DRIFTS analysis for this mode of bonding using acetylene as a probe molecule.[49] While there is no clear consensus regarding structure sensitivity in alkyne hydrogenation, there is some evidence that the geometric and electronic properties of nano-scale Au can influence phenylacetylene hydrogenation, where smaller Au size favours higher activity and styrene selectivity.[18] Nikolaev and Smirnov[17] have proposed a preferential adsorption of phenylacetylene relative to styrene on Au edge and corner sites that are prevalent with decreasing Au particle size. DFT calculations have demonstrated stronger interaction of propyne (compared with propylene) with nano-sized Au, resulting in high (80–90%) associated selectivity to propylene in the hydrogenation of propyne+propylene mixtures over Au/CeO_2.[47] Moreover, Jia *et al.* have recorded greater acetylene uptake than ethylene on Au/Al_2O_3, which was linked to enhanced (by a factor of 2000) acetylene hydrogenation rates.[45]

3.2 Pd/Al_2O_3

3.2.1 Catalyst Characteristics

The commercial Pd/Al_2O_3 sample used as benchmark exhibited comparable BET area and pore volume with a higher mean pore size when compared with the laboratory synthesised

Au/Al_2O_3 (Table 1). The TPR profile (Fig. 4(A)) presents a single negative (H_2 release) peak at 355 K that can be attributed to the decomposition of *β*-Pd hydride, which is generated by H_2 absorption at partial pressure in excess of 0.02 atm;[50-52] a pressure of 0.05 atm was used in this study. Hydride composition (H/Pd) is dependent on Pd particle size[53,54] and the value recorded (0.1) is significantly lower than that which characterises bulk Pd (0.7),[51] suggesting the formation of Pd particles at the nano-scale. Indeed, Mendez *et al.*[55] have reported an equivalent hydride composition for 0.66% w/w Pd/Al_2O_3 with a mean Pd particle size of 2.0 nm. As in the case of Au/Al_2O_3, the XRD pattern for Pd/Al_2O_3 (not shown) did not exhibit any characteristic peak for Pd metal, suggesting Pd particle formation < 5 nm.[56] This was confirmed by TEM analysis (see representative image and size distribution histogram in Fig. 4(B)) with particles in the 1-6 nm size range and a surface area-weighted mean of 3.0 nm. Ambient temperature H_2 chemisorption on Pd/Al_2O_3 was significantly greater than that recorded for Au/Al_2O_3 (Table 1), which agrees with the general consensus that a higher activation barrier exists for H_2 chemisorption on Au relative to group 10 metals.[40] In contrast to Au/Al_2O_3, H_2 chemisorption on Pd/Al_2O_3 was suppressed at the higher temperature, an effect that has been reported for Pd,[57] Pt[40,58] and Rh[59] systems. As H_2 dissociation on Pd is exothermic, elevated temperatures serve to limit uptake[39,40] whereas adsorption on supported Au is an activated process, favoured by increased temperature. The XPS spectrum over the Pd 3*d* BE region is shown in Fig. 4(C) and the associated BE value (for $3d_{5/2}$) is given in Table 1. The Pd $3d_{5/2}$ core level BE (334.9 eV) is 0.4 eV lower than the metallic Pd reference (335.3 eV),[60] suggesting electron transfer from the support to generate $Pd^{\delta-}$, which is consistent with the literature [61,62].[61,62]

3.2.2 Catalytic Response

Representative time on-stream conversion profiles are given in the inset to Fig. 2, where a temporal decrease in conversion is again evident. The experimentally determined *TOF* values, which far exceed those obtained with Au/Al_2O_3, exhibited an increase at elevated reaction temperature (Table 2). The high activity exhibited by supported Pd has been exploited in industrial catalysis for alkyne hydrogenation[47,63] and application in acetylene hydrogenation has been considered to a far greater extent than the conversion of phenylacetylene.[12,44] Supported Pd in the metallic state has been proposed as the active site for C≡C hydrogenation[47,63] where activity and selectivity in conversion of phenylacetylene has shown a dependence on Pd particle size.[64] We should note that structure "insensitivity" has also been reported for reaction over pumice supported Pd.[65] The greater rate delivered by Pd/Al_2O_3 can be attributed to increased reactive surface hydrogen as established from the chemisorption measurements (Table 1). In order to probe this effect further, phenylacetylene hydrogenation over Pd/Al_2O_3 was conducted at lower H_2 partial pressure, corresponding to an inlet molar H_2/phenylacetylene = 1, which should serve to limit the available hydrogen for reaction. The resultant *TOF* (0.11 s^{-1} at 473 K) approached that recorded for Au/Al_2O_3 (at H_2 partial pressure = 0.87 atm, Table 2), demonstrating the critical role of hydrogen activation.

Reaction over Pd/Al_2O_3 was non-selective with significant ethylbenzene formation that was favoured by higher temperature and increasing conversion, as shown in Fig. 3(A). A comparison of selectivity in the sequential/parallel reaction mechanism that applies here (Fig. 2) is only meaningful at a common level of conversion (x = 0.1 in Table 2), which establishes enhanced selectivity to styrene over Au/Al_2O_3. Conversion of a styrene feed over Pd/Al_2O_3

generated higher *TOF* relative to the phenylacetylene, representing a marked deviation from the catalytic response for Au/Al_2O_3 and can account for increased ethylbenzene production. Indeed, greater reactivity of styrene than phenylacetylene has been observed elsewhere for reaction over Ni[66] and Pd[12] catalysts. It is widely accepted that the conversion of alkenes to alkanes over Pd catalysts proceeds at a greater rate than the alkyne → alkene step.[12,47,63] The capacity of Pd sites to activate both C≡C and C=C has been demonstrated by DFT calculations[47] and is quite distinct from preferential C≡C activation on Au. Moreover, the generation of $Pd^{\delta-}$ (from XPS analysis) may result in more effective interaction with styrene as a weaker Lewis base than phenylacetylene. A decrease in inlet H_2 partial pressure to a molar H_2/phenylacetylene ratio = 1 (stoichiometry for styrene formation) shifted the selectivity/activity profile to overlap with that shown by Au/Al_2O_3 in excess H_2 (Fig. 3). The lower H_2 chemisorption capacity for Au/Al_2O_3 (Table 1) must contribute to styrene selectivity by limiting the degree of consecutive hydrogenation to ethylbenzene. It should be noted that there was no detectable activity for reaction over Au/Al_2O_3 at H_2/phenylacetylene = 1. Under conditions of excess H_2, phenylacetylene conversion to ethylbenzene is facilitated by styrene activation at Pd sites. Selectivity to the alkene can, however, be imposed by limiting the H_2 supply to the stoichiometry for styrene formation. Similar enhancement in hydrogenation selectivity over Pd catalysts is also feasible by doping the catalyst (with sulfur[67] or phosphorus[68]) or inclusion of CO in the feed.[69]

In accordance with the pathways given in Fig. 2, the steps involved in phenylacetylene hydrogenation are represented by

$$C_8H_6 + 2H_2 \xrightarrow{k_1} C_8H_{10} \quad (4)$$

$$C_8H_6 + H_2 \xrightarrow{k_2} C_8H_8 \quad (5)$$

$$C_8H_8 + H_2 \xrightarrow{k_3} C_8H_{10} \quad (6)$$

and

$$\frac{dN_{C_8H_6}}{d\left(n/F_{C_8H_6}\right)} = -\left(k_1 + k_2\right) \times N_{C_8H_6} \quad (7)$$

$$\frac{dN_{C_8H_8}}{d\left(n/F_{C_8H_6}\right)} = k_2 \times N_{C_8H_6} - k_3 \times N_{C_8H_8} \quad (8)$$

$$\frac{dN_{C_8H_{10}}}{d\left(n/F_{C_8H_6}\right)} = k_3 \times N_{C_8H_8} + k_1 \times N_{C_8H_6} \quad (9)$$

where N_i represents the molar fraction of the ith compound and k_j is the pseudo-first order rate constant of step j. From a combination of Eqs (7) and (8)

$$\frac{dN_{C_8H_8}}{dN_{C_8H_6}} = -L + M \times \left(\frac{N_{C_8H_8}}{N_{C_8H_6}}\right) \quad (10)$$

with

$$L = \frac{k_2}{k_1 + k_2} \quad \therefore \quad M = \frac{k_3}{k_1 + k_2}$$

which when integrated gives

$$N_{C_8H_8} = \frac{L}{1-M} \times \left(N_{C_8H_6}{}^{M} - N_{C_8H_6}\right) + C \quad (11)$$

where C is a constant and the values of L and M can be determined by non-linear mathematical fitting. The applicability of this parallel/consecutive mechanism can be assessed from the entries in Fig. 3(B), where it can be seen that the model provides a more than adequate fit to the experimental data. The rate constant ratios (k_1/k_2 and k_3/k_2) obtained from the L and M parameters are given in Table 2 for Au/Al_2O_3 and Pd/Al_2O_3 at the two reaction temperatures. A strictly consecutive reaction network should yield a value of L close to unity ($k_1 = 0$) where lower L values reflect increased contribution due to the direct conversion of phenylacetylene to

ethyl benzene. Reaction over Au/Al_2O_3 at 353 K proceeded in a predominantly stepwise fashion (*L* approaching unity) where the high styrene selectivity results from the far lower rate of subsequent hydrogenation ($k_2 >> k_3$). Stepwise hydrogenation was also favoured at the higher reaction temperature (*L* = 0.99) but styrene hydrogenation was promoted to a greater extent (marked increase in k_3/k_2), which can explain the observed ethylbenzene formation. In the case of Pd/Al_2O_3, phenylacetylene hydrogenation followed consecutive steps at 353 K but, in contrast to Au/Al_2O_3, the rate of styrene hydrogenation far exceeded the phenylacetylene → styrene step resulting in significant ethylbenzene production. Reaction at 473 K favoured a concerted conversion of ethylbenzene ($k_1 \approx k_2$) and styrene reduction ($k_3 >> k_2$) leading to increased ethylbenzene selectivity (Fig. 3 and Table 2). It should be noted that single step direct phenylacetylene → ethylbenzene has been proposed for reaction over Pd/pumice[65] and Pd/C.[44] Operation at H_2/phenylacetylene = 1 (at 473 K) over Pd/Al_2O_3 generated $k_1/k_2 = 0.05$ and $k_3/k_2 = 1.14$, which approaches the values recorded for Au/Al_2O_3 (see Table 2). Selectivity exhibited by Au/Al_2O_3 can be linked to the preferential adsorption/activation of phenylacetylene and lower reactivity of styrene. In contrast, both phenylacetylene and styrene are activated on Pd/Al_2O_3 where the alkene exhibits higher reactivity but selectivity can be tuned by altering the inlet H_2/phenylacetylene.

4. Conclusions

We have established a distinct catalytic response for alumina supported Au and Pd in the gas phase continuous hydrogenation of phenylacetylene. Charge transfer from Al_2O_3 to nano-scale Au (2-8 nm) and Pd (1-6 nm) generates an electron rich metal phase. Pd/Al_2O_3 exhibited a greater capacity for H_2 uptake under reaction conditions and delivered an

appreciably higher *TOF*. Kinetic analysis has revealed stepwise phenylacetylene hydrogenation in excess H_2 over Au/Al_2O_3 with 100% selectivity to styrene at 353 K that is attributed to preferential adsorption/activation of phenylacetylene relative to styrene and further hydrogenation is limited by the available surface hydrogen. An increase in temperature (to 473 K) raised *TOF* with the promotion of sequential styrene hydrogenation to ethylbenzene. Stepwise hydrogenation also prevailed over Pd/A_2O_3 at the lower temperature but surface activation of styrene coupled with enhanced H_2 dissociation generated significant ethylbenzene. Increased reaction temperature favoured parallel direct phenylacetylene hydrogenation with increased ethylbenzene selectivity. Lowering the inlet H_2/phenylacetylene ratio to 1 delivered an activity/selectivity response over Pd/A_2O_3 approaching that for Au/A_2O_3, demonstrating the critical role of hydrogen supply in determining catalyst performance.

Acknowledgements

EPSRC support for free access to the TEM/SEM facility at the University of St Andrews and financial support (to X. Wang) through the Overseas Research Students Award Scheme (ORSAS) are also acknowledged.

References

1 Arena, F, Cum, G, Gallo, R, and Parmaliana, A, Palladium catalysts supported on oligomeric aramides in the liquid-phase hydrogenation of phenylacetylene. *J Mol Catal A Chem* **110**:235-242 (1996).

2 Domínguez-Domínguez, S, Berenguer-Murcia, A, Cazorla-Amorós, D, and Linares-Solano, A, Semihydrogenation of phenylacetylene catalyzed by metallic nanoparticles containing noble metals. *J Catal* **243**:74-81 (2006).

3 Li, C, Shao, Z, Pang, M, Williams, CT, and Liang, C, Carbon nanotubes supported Pt catalysts for phenylacetylene hydrogenation: effects of oxygen containing surface groups on Pt dispersion and catalytic performance. *Catal Today* **186**:69-75 (2012).

4 Dominguez-Dominguez, S, Berenguer-Murcia, A, Pradhan, BK, Linares-Solano, A, and Cazorla-Amoros, D, Semihydrogenation of phenylacetylene catalyzed by palladium nanoparticles supported on carbon materials. *J Phys Chem C* **112**:3827-3834 (2008).

5 Bacchi, A, Carcelli, M, Costa, M, Leporati, A, Leporati, E, Pelagatti, P, Pelizzi, C, and Pelizzi, G, Palladium(II) complexes containing a P, N chelating ligand part II. synthesis and characterisation of complexes with different hydrazinic ligands. catalytic activity in the hydrogenation of double and triple C-C bonds. *J Organomet Chem* **535**:107-120 (1997).

6 Dominguez-Dominguez, S, Berenguer-Murcia, A, Linares-Solano, A, and Cazorla-Amoros, D, Inorganic materials as supports for palladium nanoparticles: application in the semi-hydrogenation of phenylacetylene. *J Catal* **257**:87-95 (2008).

7 Li, C, Shao, Z, Pang, M, Williams, CT, Zhang, X, and Liang, C, Carbon nanotubes supported mono- and bimetallic Pt and Ru catalysts for selective hydrogenation of phenylacetylene. *Ind Eng Chem Res* **51**:4934-4941 (2012).

8 Quek, X-Y, Guan, Y, and Hensen, EJM, Structure sensitivity in the hydrogenation of unsaturated hydrocarbons over Rh nanoparticles. *Catal Today* **183**:72-78 (2012).

9 Navalikhina, MD, Kavalerskaya, NE, Lokteva, ES, Peristyi, AA, Golubina, EV, and Lunin, VV, Selective hydrogenation of phenylacetylene on Ni and Ni-Pd catalysts modified with heteropoly compounds of the Keggin type. *Russ J Phys Chem A* **86**:1800-1807 (2012).

10 Yu, J-W, Wang, X-Y, Yuan, C-Y, Li, W-Z, Wang, Y-H, and Zhang, Y-W, Synthesis of ultrathin Ni nanosheets for semihydrogenation of phenylacetylene to styrene under mild conditions. *Nanoscale* **10**:6936-6944 (2018).

11 Vergunst, T, Kapteijn, F, and Moulijn, JA, Optimization of geometric properties of a monolithic catalyst for the selective hydrogenation of phenylacetylene. *Ind Eng Chem Res* **40**:2801-2809 (2001).

12 Liu, W, Otero Arean, C, Bordiga, S, Groppo, E, and Zecchina, A, Selective phenylacetylene hydrogenation on a polymer-supported palladium catalyst monitored by FTIR spectroscopy. *ChemCatChem* **3**:222-226 (2011).

13 Goršek, A, and Glavič, P, Design of batch versus continuous processes: part I:

single-purpose equipment. *Chem Eng Res Des* **75**:709-717 (1997).

14 Wang, W, Zheng, Y, Lin, J, She, Y, and Fu, KJ, Time-resolved IR study of gas-phase reactions of benzene with Group VIB metal pentacarbonyls and tetracarbonyls. *J Phys Chem* **97**:11921-11928 (1993).

15 Goossens, A, Schoonman, J, and Yoshimura, M, Gas-phase synthesis of nano-structured semiconductors. *Eur J Solid State Inorg Chem* **32**:779-786 (1995).

16 Laerdahl, JK, and Uggerud, E, Gas phase nucleophilic substitution. *Int J Mass Spectrom* **214**:277-314 (2002).

17 Nikolaev, SA, and Smirnov, VV, Synergistic and size effects in selective hydrogenation of alkynes on gold nanocomposites. *Catal Today* **147**:S336-S341 (2009).

18 Nikolaev, S, and Smirnov, V, Selective hydrogenation of phenylacetylene on gold nanoparticles. *Gold Bull* **42**:182-189 (2009).

19 Nikolaev, S, Permyakov, N, Smirnov, V, Vasil'kov, A, and Lanin, S, Selective hydrogenation of phenylacetylene into styrene on gold nanoparticles. *Kinet Catal* **51**:288-292 (2010).

20 Wang, X, Perret, N, and Keane, MA, The role of hydrogen partial pressure in the gas phase hydrogenation of p-chloronitrobenzene over alumina supported Au and Pd: a consideration of reaction thermodynamics and kinetics. *Chem Eng J* **210**:103-113 (2012).

21 Wang, X, Perret, N, Delgado, JJ, Blanco, G, Chen, X, Olmos, CM, Bernal, S, and Keane, MA, Reducible support effects in the gas phase hydrogenation of p-chloronitrobenzene over gold. *J Phys Chem C* **117**:994-1005 (2013).

22 Wang, X, Perret, N, and Keane, MA, Gas phase hydrogenation of nitrocyclohexane over supported gold catalysts. *Appl Catal A Gen* **467**:575-584 (2013).

23 Li, M, Wang, X, Cárdenas-Lizana, F, and Keane, MA, Effect of support redox character on catalytic performance in the gas phase hydrogenation of benzaldehyde and nitrobenzene over supported gold. *Catal Today* **279**:19-28 (2017).

24 Mastalir, A, Kiraly, Z, and Berger, F, Comparative study of size-quantized Pd-montmorillonite catalysts in liquid-phase semihydrogenations of alkynes. *Appl Catal A Gen* **269**:161-168 (2004).

25 Starodubtseva, EV, Vinogradov, MG, Turova, OV, Bumagin, NA, Rakov, EG, and

Sokolov, VI, Palladium(0) supported on carbon nanotubes as an efficient catalyst of the CC bond hydrogenation. *Catal Commun* **10**:1441-1442 (2009).

26 Weerachawanasak, P, Mekasuwandumrong, O, Arai, M, Fujita, S-I, Praserthdam, P, and Panpranot, J, Effect of strong metal-support interaction on the catalytic performance of Pd/TiO_2 in the liquid-phase semihydrogenation of phenylacetylene. *J Catal* **262**:199-205 (2009).

27 Panpranot, J, Phandinthong, K, Sirikajorn, T, Arai, M, and Praserthdam, P, Impact of palladium silicide formation on the catalytic properties of Pd/SiO_2 catalysts in liquid-phase semihydrogenation of phenylacetylene. *J Mol Catal A Chem* **261**:29-35 (2007).

28 Keane, MA, Gas phase hydrogenation/hydrogenolysis of benzaldehyde and o-tolualdehyde over Ni/SiO_2. *J Mol Catal A Chem* **118**:261-269 (1997).

29 Tavoularis, G, and Keane, MA, The gas phase hydrodechlorination of chlorobenzene over nickel/silica. *J Chem Technol Biotechnol* **74**:60-70 (1999).

30 Yuan, G, and Keane, MA, Aqueous-phase hydrodechlorination of 2,4-dichlorophenol over Pd/Al_2O_3: Reaction under controlled pH. *Ind Eng Chem Res* **46**:705-715 (2007).

31 Zhang, Z, and Pinnavaia, TJ, Mesoporous γ-alumina formed through the surfactant-mediated scaffolding of peptized pseudoboehmite nanoparticles. *Langmuir* **26**:10063-10067 (2010).

32 Trueba, M, and Trasatti, SP, γ-Alumina as a support for catalysts: a review of fundamental aspects. *Eur J Inorg Chem* **2005**:3393-3403 (2005).

33 Cárdenas-Lizana, F, Gómez-Quero, S, Jacobs, G, Ji, Y, Davis, BH, Kiwi-Minsker, L, and Keane, MA, Alumina supported Au-Ni: surface synergism in the gas phase hydrogenation of nitro-compounds. *J Phys Chem C* **116**:11166-11180 (2012).

34 Costello, CK, Guzman, J, Yang, JH, Wang, YM, Kung, MC, Gates, BC, and Kung, HH, Activation of $Au/\gamma\text{-}Al_2O_3$ catalysts for CO oxidation: characterization by X-ray absorption near edge structure and temperature programmed reduction. *J Phys Chem B* **108**:12529-12536 (2004).

35 Baron, M, Bondarchuk, O, Stacchiola, D, Shaikhutdinov, S, and Freund, HJ, Interaction of gold with cerium oxide supports: CeO_2(111) thin films vs CeOx nanoparticles. *J Phys Chem C* **113**:6042-6049 (2009).

36 Wang, F, and Lu, G, Control reaction path of CO oxidation by regulating the oxidation state of Au species. *Catal Lett* **134**:72-77 (2010).

37 Perret, N, Wang, X, Delannoy, L, Potvin, C, Louis, C, and Keane, MA, Enhanced selective nitroarene hydrogenation over Au supported on β-Mo_2C and β-Mo_2C/Al_2O_3. *J Catal* **286**:172-183 (2012).

38 Boronat, M, Concepción, P, Corma, A, González, S, Illas, F, and Serna, P, A molecular mechanism for the chemoselective hydrogenation of substituted nitroaromatics with nanoparticles of gold on TiO_2 Catalysts: a cooperative effect between gold and the support. *J Am Chem Soc* **129**:16230-16237 (2007).

39 Bus, E, Miller, JT, and van Bokhoven, JA, Hydrogen chemisorption on Al_2O_3-supported gold catalysts. *J Phys Chem B* **109**:14581-14587 (2005).

40 Bond, GC, Louis, C, and Thompson, DT. (2006), Catalysis by gold, Imperial College Press, London

41 Wang, X, Hao, Y, and Keane, MA, Selective gas phase hydrogenation of p-nitrobenzonitrile to p-aminobenzonitrile over zirconia supported gold. *Appl Catal A Gen* **510**:171-179 (2016).

42 Kartusch, C, and van Bokhoven, J, Hydrogenation over gold catalysts: the interaction of gold with hydrogen. *Gold Bull* **42**:343-348 (2009).

43 Lin, S, and Vannice, MA, Gold dispersed on TiO_2 and SiO_2: adsorption properties and catalytic behavior in hydrogenation reactions. *Catal Lett* **10**:47-61 (1991).

44 Jackson, SD, and Shaw, LA, The liquid-phase hydrogenation of phenyl acetylene and styrene on a palladium/carbon catalyst. *Appl Catal A Gen* **134**:91-99 (1996).

45 Jia, J, Haraki, K, Kondo, JN, Domen, K, and Tamaru, K, Selective hydrogenation of acetylene over Au/Al_2O_3 catalyst. *J Phys Chem B* **104**:11153-11156 (2000).

46 Gluhoi, AC, Bakker, JW, and Nieuwenhuys, BE, Gold, still a surprising catalyst: selective hydrogenation of acetylene to ethylene over Au nanoparticles. *Catal Today* **154**:13-20 (2010).

47 Segura, Y, Lopez, N, and Perez-Ramirez, J, Origin of the superior hydrogenation selectivity of gold nanoparticles in alkyne + alkene mixtures: Triple- versus double-bond activation. *J Catal* **247**:383-386 (2007).

48 Schimpf, S, Lucas, M, Mohr, C, Rodemerck, U, Brückner, A, Radnik, J, Hofmeister, H,

and Claus, P, Supported gold nanoparticles: in-depth catalyst characterization and application in hydrogenation and oxidation reactions. *Catal Today* **72**:63-78 (2002).

49 Ivanov, AV, Koklin, AE, Uvarova, EB, and Kustov, LM, A DRIFT spectroscopic study of acetylene adsorbed on metal oxides. *Phys Chem Chem Phys* **5**:4718-4723 (2003).

50 Gopinath, R, Seshu Babu, N, Vinod Kumar, J, Lingaiah, N, and Sai Prasad, P, Influence of Pd precursor and method of preparation on hydrodechlorination activity of alumina supported palladium catalysts. *Catal Lett* **120**:312-319 (2008).

51 Gómez-Quero, S, Cárdenas-Lizana, F, and Keane, MA, Effect of metal dispersion on the liquid-phase hydrodechlorination of 2,4-dichlorophenol over Pd/Al_2O_3. *Ind Eng Chem Res* **47**:6841-6853 (2008).

52 Babu, NS, Lingaiah, N, Gopinath, R, Sankar Reddy, PS, and Sai Prasad, PS, Characterization and reactivity of alumina-supported Pd catalysts for the room-temperature hydrodechlorination of chlorobenzene. *J Phys Chem C* **111**:6447-6453 (2007).

53 Nag, NK, A study on the formation of palladium hydride in a carbon-supported palladium catalyst. *J Phys Chem B* **105**:5945-5949 (2001).

54 Fagherazzi, G, Benedetti, A, Polizzi, S, Mario, A, Pinna, F, Signoretto, M, and Pernicone, N, Structural investigation on the stoichiometry of β-PdHx in Pd/SiO_2 catalysts as a function of metal dispersion. *Catal Lett* **32**:293-303 (1995).

55 Mendez, CM, Olivero, H, Damiani, DE, and Volpe, MA, On the role of Pd β-hydride in the reduction of nitrate over Pd based catalyst. *Appl Catal B Environ* **84**:156-161 (2008).

56 Kim, DH, Chin, Y-H, Muntean, GG, Yezeretz, A, Currier, NW, Epling, WS, Chen, H-Y, Hess, H, and Peden, CHF, Relationship of Pt particle size to the NOx storage performance of thermally aged $Pt/BaO/Al_2O_3$ Lean NOx trap catalysts. *Ind Eng Chem Res* **45**:8815-8821 (2006).

57 Bhat, VV, Contescu, CI, and Gallego, NC, Kinetic effect of Pd additions on the hydrogen uptake of chemically-activated ultramicroporous carbon. *Carbon* **48**:2361-2364 (2010).

58 Bus, E, and van Bokhoven, JA, Hydrogen chemisorption on supported platinum, gold, and platinum-gold-alloy catalysts. *Phys Chem Chem Phys* **9**:2894-2902 (2007).

59 Lu, C-M, Wang, I, Chou, S-C, and Yeh, C-T, Hydrogenation of benzene over rhodium-copper alloy crystallites supported on alumina. *Chinyi J.* **19**:119-131 (2001).

60 Liu, H, Liang, M, Xiao, C, Zheng, N, Feng, X, Liu, Y, Xie, J, and Wang, Y, An excellent Pd-based nanocomposite catalyst for the selective hydrogenation of para-chloronitrobenzene. *J Mol Catal A Chem* **308**:79-86 (2009).

61 Sun, K, Liu, J, Nag, N, and Browning, ND, Studying the metal-support interaction in Pd/γ-Al_2O_3 Catalysts by atomic-resolution electron energy-loss spectroscopy. *Catal Lett* **84**:193-199 (2002).

62 Tsud, N, Johanek, V, Stara, I, Veltruska, K, and Matolin, V, CO adsorption on palladium model catalysts: XPS Pd/Al_2O_3 interaction study. *Surf Sci* **467**:169-176 (2000).

63 Borodzinski, A, and Bond, GC, Selective hydrogenation of ethyne in ethene-rich streams on palladium catalysts. part 1. effect of changes to the catalyst during reaction. *Catal Rev* **48**:91-144 (2006).

64 Carturan, G, Facchin, G, Cocco, G, Enzo, S, and Navazio, G, Influence of metal dispersion on selectivity and kinetics of phenylacetylene hydrogenation catalyzed by supported palladium. *J Catal* **76**:405-417 (1982).

65 Duca, D, Liotta, LF, and Deganello, G, Selective hydrogenation of phenylacetylene on pumice-supported palladium catalysts. *J Catal* **154**:69-79 (1995).

66 Chen, X, Zhao, A, Shao, Z, Li, C, Williams, CT, and Liang, C, Synthesis and catalytic properties for phenylacetylene hydrogenation of silicide modified nickel catalysts. *J Phys Chem C* **114**:16525-16533 (2012).

67 Liu, Y, McCue, AJ, Feng, J, Guan, S, Li, D, and Anderson, JA, Evolution of palladium sulfide phases during thermal treatments and consequences for acetylene hydrogenation. *J Catal* **364**:204-215 (2018).

68 Liu, Y, McCue, AJ, Miao, C, Feng, J, Li, D, and Anderson, JA, Palladium phosphide nanoparticles as highly selective catalysts for the selective hydrogenation of acetylene. *J Catal* **364**:406-414 (2018).

69 McKenna, FM, Mantarosie, L, Wells, RPK, Hardacre, C, and Anderson, JA, Selective hydrogenation of acetylene in ethylene rich feed streams at high pressure over ligand modified Pd/TiO_2. *Catal Sci Tech* **2**:632-638 (2012).

Table 1: Physicochemical characteristics of Au/Al_2O_3 and Pd/Al_2O_3.

Catalyst	Metal loading (% w/w)	TPR T_{max} (K)	BET area ($m^2\ g^{-1}$)	Pore volume/mean size ($cm^3\ g^{-1}$)/(nm)	H_2 chemisorption (μmol g^{-1})	Mean particle size/range (nm)	XPS BE (eV)
Au/Al_2O_3	1.1	458	166	0.36/5.8	0.4[b]/4.4[c]	4.3/2-8	83.4[d]
Pd/Al_2O_3	1.2	355[a]	156	0.46/9.2	33.8[b]/22.6[c]	3.0/1-6	334.9[e]

[a]associated with H_2 release in Pd hydride decomposition; [b]at 298 K; [c]at 423 K; [d]Au $4f_{7/2}$; [e]Pd $3d_{5/2}$

Table 2: Temperature dependence of turnover frequency (*TOF*), associated selectivities (*S*) at a common fractional conversion ($x = 0.1$), values of the *L* and *M* parameters and rate constant ratios (k_1/k_2 and k_3/k_2 see Fig. 2) obtained from the fit (see Eqs (7)-(11) and Fig. 3(B)) of product composition from phenylacetylene and styrene reaction over Au/Al_2O_3 and Pd/Al_2O_3.

Catalyst	Temperature (K)	Phenylacetylene feed						Styrene feed	
		TOF (s^{-1})	*S* (%)	*L*	*M*	k_1/k_2	k_3/k_2	*TOF* (s^{-1})	*S* (%)[a]
Au/Al_2O_3	353	1.5×10^{-2}	styrene (100)	0.93	0.07	0.07	0.08	7×10^{-4}	100
Au/Al_2O_3	473	13×10^{-2}	styrene (90); ethylbenzene (10)	0.99	0.83	0.01	0.84	9×10^{-3}	100
Pd/Al_2O_3	353	0.9	styrene: (88); ethylbenzene (12)	0.99	2.54	0.01	2.57	22	100
Pd/Al_2O_3	473	5.6	styrene (82); ethylbenzene (18)	0.51	2.51	0.94	4.87	28	100

[a]ethyl benzene was the only product

Figure Captions

Fig. 1: Au/Al_2O_3 characteristics: (A) TPR profile, (B) XPS spectrum over the Au 4*f* BE region and (C) representative STEM image (inset) with associated Au particle size (*d*) distribution histogram.

Fig. 2: (A): Reaction pathways in the hydrogenation of phenylacetylene. (B): variation of phenylacetylene fractional conversion (x) with time-on-stream over Au/Al_2O_3 (■: n/F = 9.3×10^{-3} h, □: $n/F = 1.4 \times 10^{-3}$ h) and Pd/Al_2O_3 (●: $n/F = 9.4 \times 10^{-5}$ h, ○: $n/F = 4.7 \times 10^{-5}$ h) at 353 K (solid symbols) and 473 K (open symbols): H_2/phenylacetylene > 60; lines represent fit to eq. (3).

Fig. 3: (A): Variation of styrene selectivity (S) with phenylacetylene fractional conversion (x) over Au/Al_2O_3 (■, □) and Pd/Al_2O_3 (●, ○) at 353 K (solid symbols) and 473 K (open symbols), where H_2/phenylacetylene > 60. Note: × represents S over Pd/Al_2O_3 at 473 K where molar H_2/phenylacetylene = 1. (B) Dependence of styrene mole fraction (N_{C8H8}) on phenylacetylene mole fraction (N_{C8H6}) for reaction over Au/Al_2O_3 and Pd/Al_2O_3 (symbols as above); lines represent fit to the consecutive/parallel mechanism (see Eqs (7)-(11), $R^2 > 0.98$).

Fig. 4: Pd/Al_2O_3 characteristics: (A) TPR profile, (B) representative TEM image (inset) with associated particle size (*d*) histogram and (C) XPS spectrum over Pd 3*d* BE region.

Fig. 1

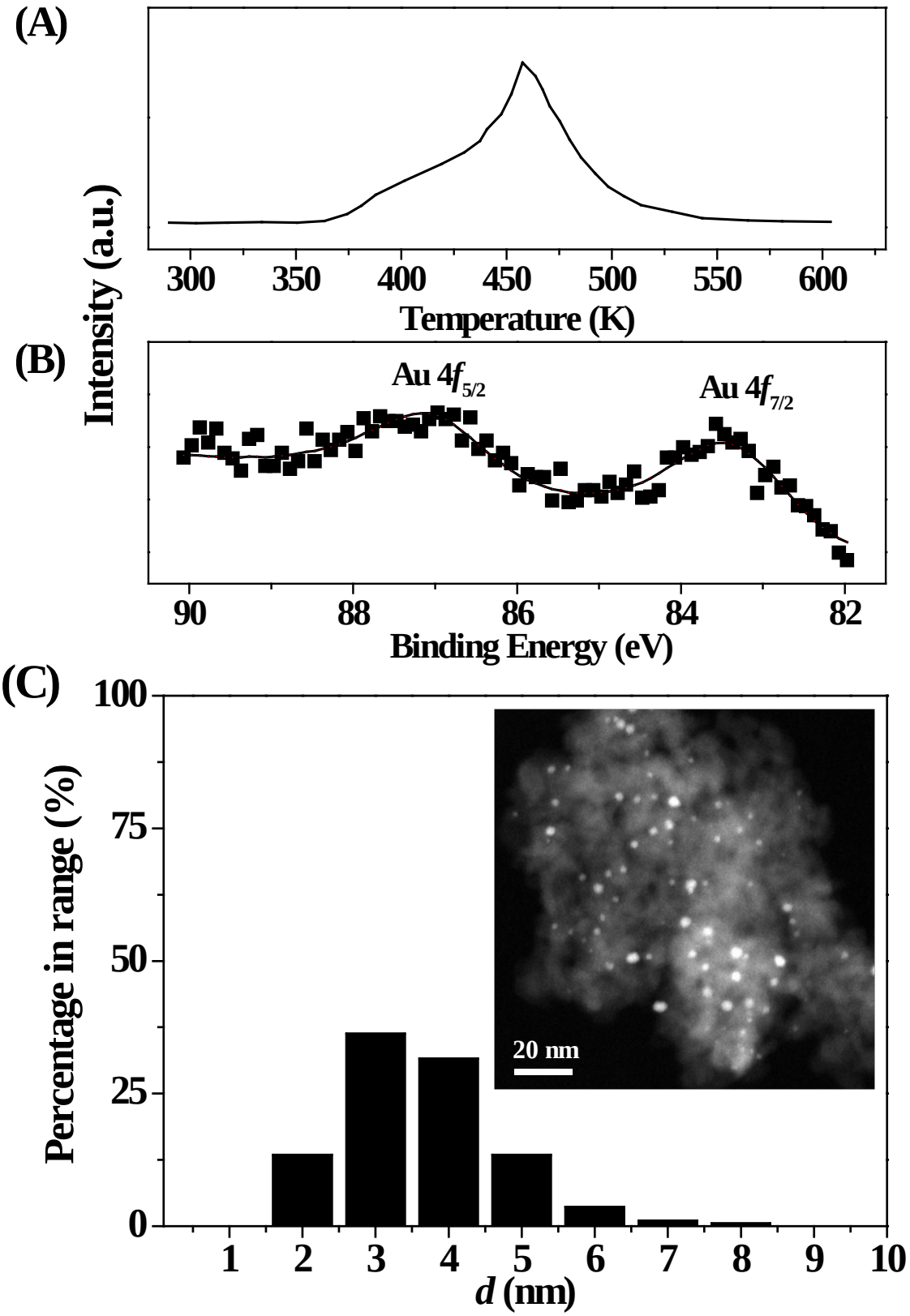
(A)
Intensity (a.u.)
300
350
400
450
500
550
600
Temperature (K)
(B)
Au 4f5/2
Au 4f7/2
90
88
86
84
82
Binding Energy (eV)
(C)
Percentage in range (%)
100
75
50
25
0
20 nm
1
2
3
4
5
6
7
8
9
10
d (nm)

Fig. 2

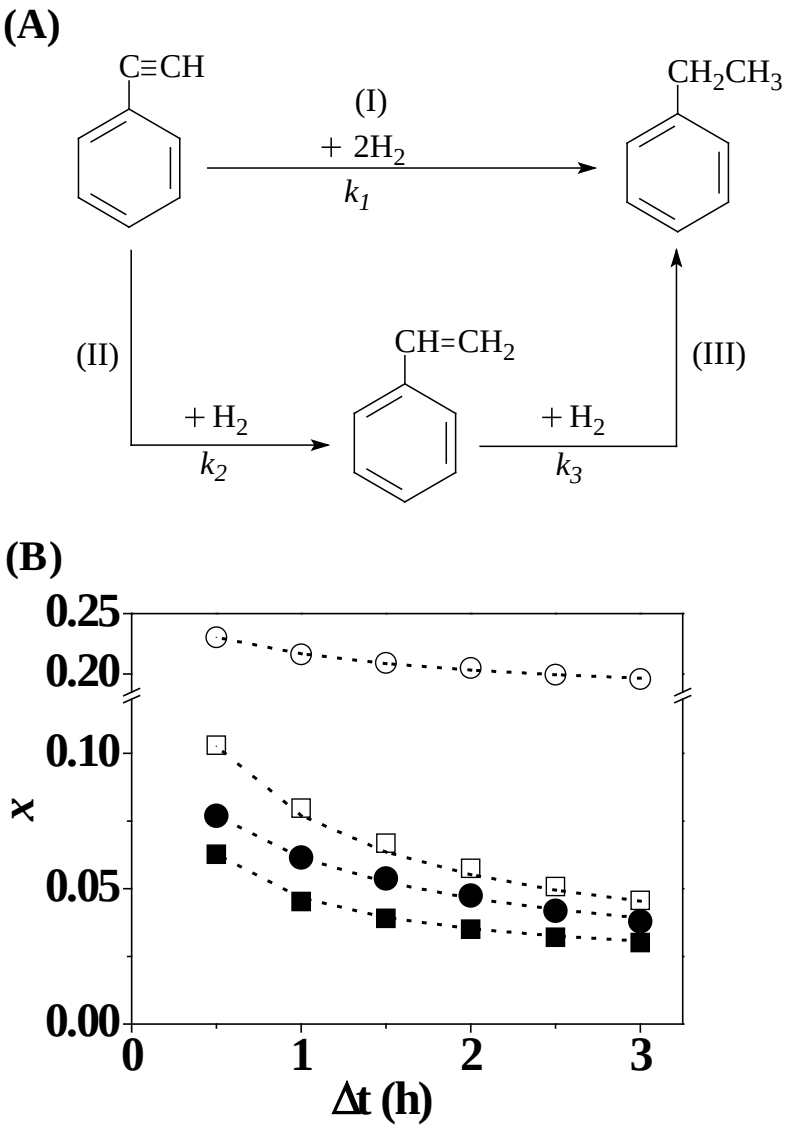
(A)
C≡CH
(I)
+ 2H2
k1
CH2CH3
(II)
CH=CH2
(III)
+ H2
k2
+ H2
k3
(B)
0.25
0.20
0.10
0.05
0.00
x
0
1
2
3
Δt (h)

Fig. 3

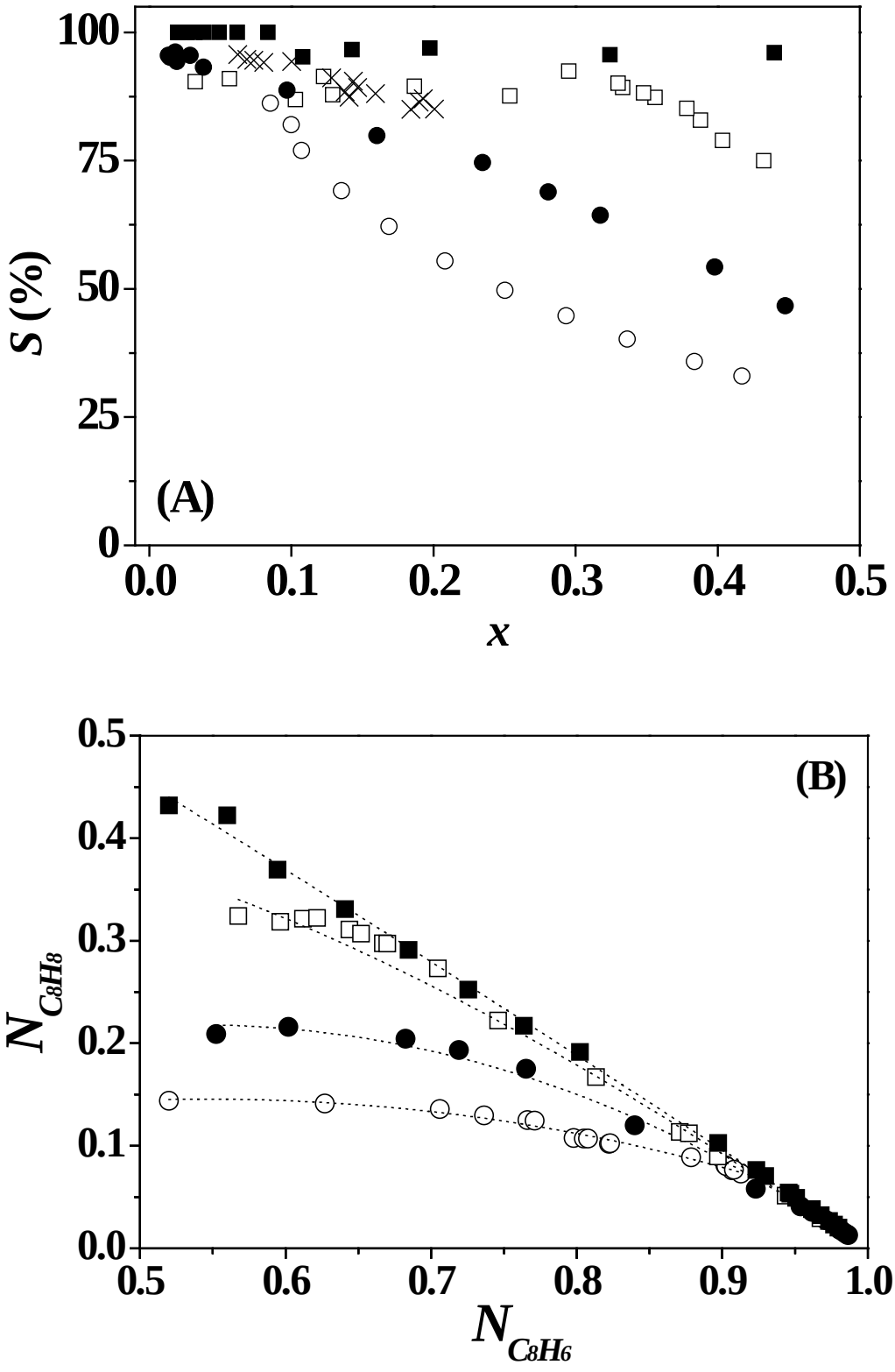
100
75
50
25
0
S (%)
(A)
0.0
0.1
0.2
0.3
0.4
0.5
x
0.5
0.4
0.3
0.2
0.1
0.0
N C8H8
(B)
0.5
0.6
0.7
0.8
0.9
1.0
N C8H6

Fig. 4

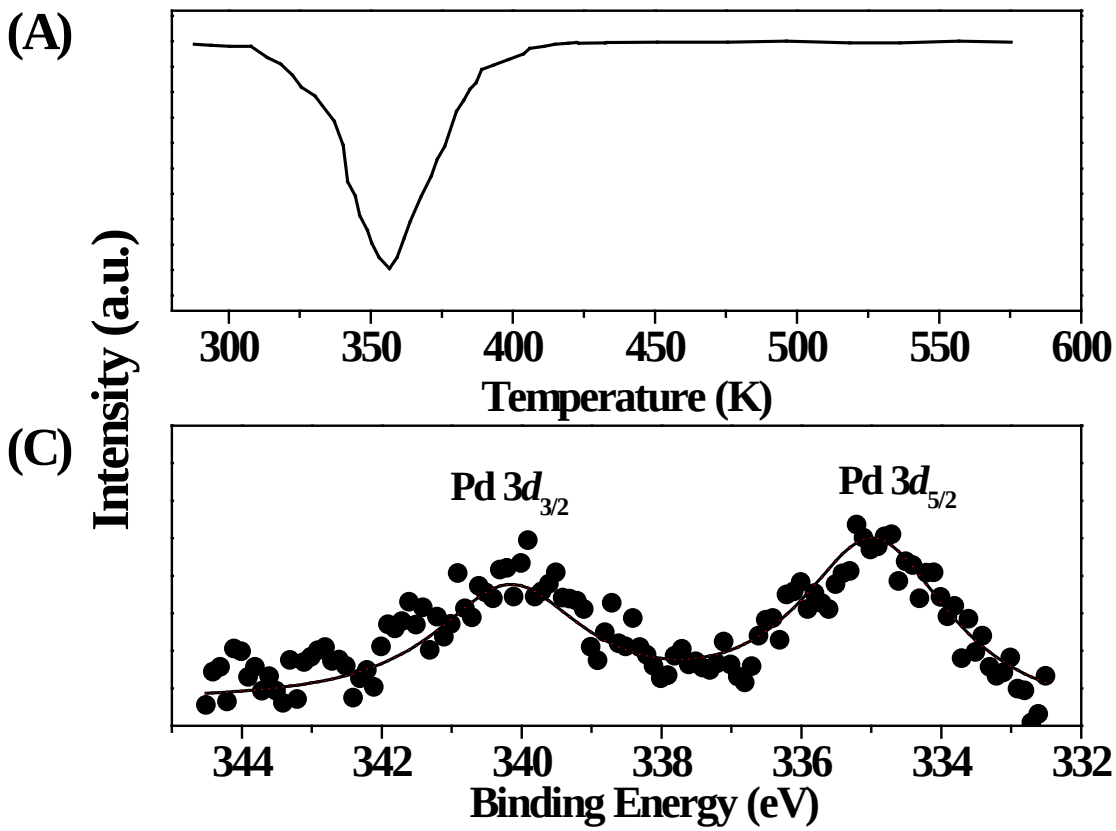
(A)
Intensity (a.u.)
300
350
400
450
500
550
600
Temperature (K)
(C)
Pd 3$d_{3/2}$
Pd 3$d_{5/2}$
344
342
340
338
336
334
332
Binding Energy (eV)

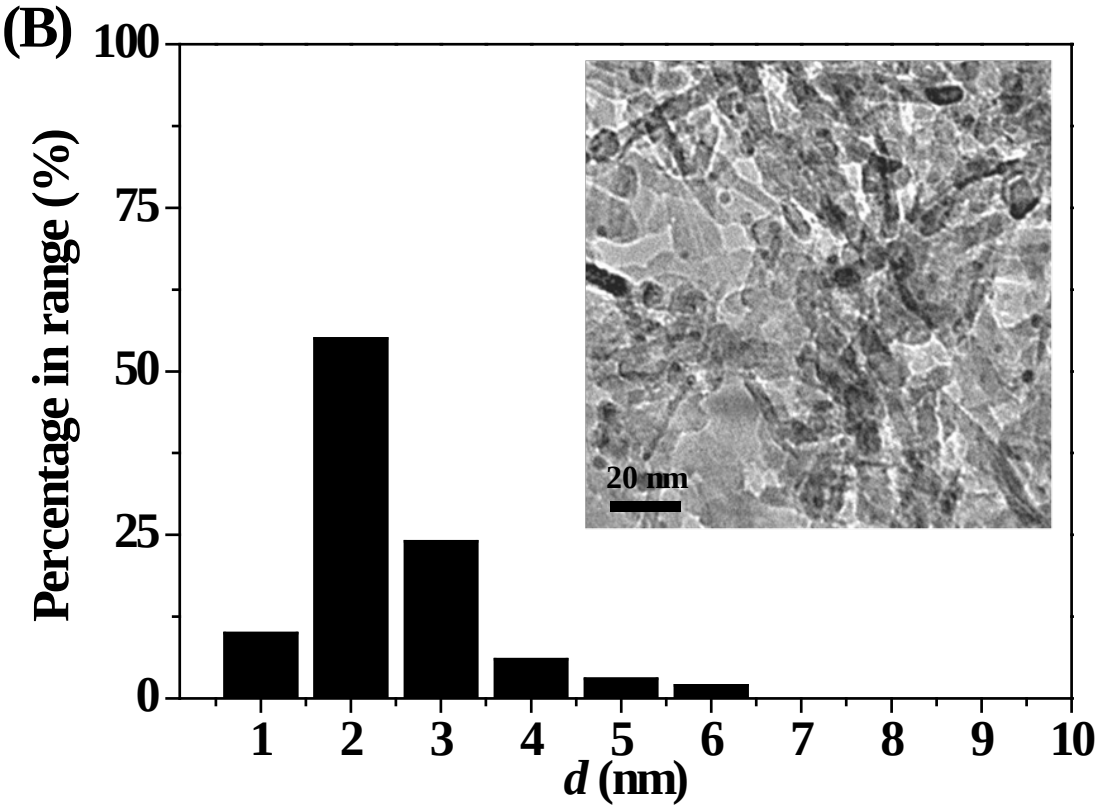
(B)
Percentage in range (%)
100
75
50
25
0
1
2
3
4
5
6
7
8
9
10
d (nm)
20 nm